NASA CONTRACTOR REPORT

NASA CR-574

NASA CR-574

ON THE USE OF FILAMENT WOUND TOROIDS AS PNEUMATIC SHOCK ABSORBERS

by Richard H. MacNeal and Julius Loisch

Prepared by
ASTRO RESEARCH CORPORATION
Santa Barbara, Calif.
for

NATIONAL AERONAUTICS AND SPACE ADMINISTRATION • WASHINGTON, D. C. • SEPTEMBER 1966

NASA CR-574

ON THE USE OF FILAMENT WOUND TOROIDS AS PNEUMATIC SHOCK ABSORBERS

By Richard H. MacNeal and Julius Loisch

Prepared under Contract No. NASw-652 by
ASTRO RESEARCH CORPORATION
Santa Barbara, Calif.

for

NATIONAL AERONAUTICS AND SPACE ADMINISTRATION

For sale by the Clearinghouse for Federal Scientific and Technical Information
Springfield, Virginia 22151 – Price $2.00

CONTENTS

ABSTRACT

This report contains the results of a study on the use of filament wound toroids as pneumatic shock absorbers. Expressions for the specific energy absorption under isobaric and adiabatic conditions are derived and compared with the performance of competing systems. Means for improving stroke efficiency are discussed.

The stiffness properties of a compressed toroid under combined compression, bending and shear are derived analytically and compared with experimental measurements. In addition the buckling behaviour of a compressed stack of toroids is analyzed and compared with test results. In both cases the agreement between analysis and experiment is sufficiently good to validate the theory for engineering calculations.

LIST OF SYMBOLS

a	radius of polar circle of toroid
c_1, c_2	see Figure 10
E_a	absorbed energy
EI	bending stiffness
E_s	specific energy, see Eqn. (1)
F	compressive load
g	acceleration of gravity
h	compressed height of toroid
h_o	undeflected height of toroid
h_1, h_2	see Figure 11
K	ratio of specific heats
KAG	shear stiffness
ℓ	length of column
m	fixity index
M	bending moment
n	number of toroids in stack
p	pressure
p_a	ambient pressure
p_g	gage pressure
p_o	pressure at no load
r	distance from polar axis
r_1, r_2	see Figure 10
R	gas constant
s	distance along meridian
(SF)	safety factor
T	temperature

T_h	hoop tension
T_m	meridional tension
u	stroke
$\bar{u}$	ratio of stroke to undeflected height
V	volume of container, also shear force
V_o	volume of container at no load
V_s	volume of structural material
w	lateral deflection
W	weight
x	distance
α	ratio of non-structural weight to structural weight
β	angle between fibers and meridional plane
η	stroke efficiency, see Eqn. (20)
ϵ	strain
ϵ_o	strain at no load
φ	azimuth angle from load plane
ρ	density
λ	specific strength see Eqn. (3)
σ	stress
θ	rotation of cover plate, see Figure 11

1. INTRODUCTION

This report contains the results of a study on the use of filament wound toroids as pneumatic shock absorbers. The primary purpose of the study was to develop, and to confirm by careful experiment, an engineering theory for design. A secondary purpose was to establish performance goals that have a reasonable expectation of achievement in future designs and thereby to provide a basis for the evaluation of the potential capabilities of toroidal shock absorbers.

The application of flexible pneumatic shock absorbers, or gas bags, as landing gears for reentry capsules and other flight vehicles has been seriously proposed and extensively tested. Reference 1 contains an evaluation of the performance of gas bags relative to other impact absorbing devices. The major disadvantages of gas bags were considered in Reference 1 to be their inability to withstand lateral loads and their tendency to buckle. The present report presents design procedures intended to overcome these difficulties.

Reference 2 is an excellent study of the gas-dynamic aspects of landing impact absorption without, however, much consideration of structural design. References 3 through 7 present the results of tests with gas-bag impact absorbers.

Examples of the type of impact absorber considered in this report are shown in Figure 1. It consists of a toroidal rubber bladder covered by high strength structural filaments. The load is applied parallel to the polar axis. In Figure 1a the structural fibers carry meridional tension, while rings on the polar circles carry hoop tension. In Figure 1b the structural fibers carry both meridional and hoop tension by virtue of their helix angle. A multiple toroid configuration for long strokes is shown in Figure 19.

The present study is based on earlier analytical studies of filament wound pressure vessels reported in References 8, 9 and 10. The primary concern

of the earlier work was to establish precise geometrical shapes and winding patterns in order to fully exploit the strength of the structural filaments (isotensoid design). In the present study geometric shapes are treated less rigorously in order to facilitate the analysis of large deformations.

2. ENERGY DISSIPATING CHARACTERISTICS OF A TOROIDAL SHOCK ABSORBER

The performance of a shock absorber is measured in terms of several parameters, the principal ones being

- the specific energy, E_s, which is the ratio of the energy absorbed by the shock absorber to its weight.
- the stroke efficiency, η, which is the ratio of the absorbed energy to the energy that would be absorbed if the force was constant and equal to its maximum value over the entire stroke.
- the deceleration onset rate, which is the maximum rate of change of deceleration, measured in g's per second.

The specific energy and stroke efficiency of a toroidal shock absorber will be computed for a variety of conditions and compared with other types of shock absorbers. As may be seen from load-stroke curves to be presented, the deceleration onset rate of a toroidal shock absorber is inherently low.

2.1 Specific Energy

The specific energy of a shock absorber is defined by

$$E_s = \frac{\text{energy absorbed by device}}{\text{weight of device}} \qquad (1)$$

The weight of a pneumatic shock absorber includes the weight of the gas, the weight of structure used to contain the gas and to resist loads, and the weight of other necessary items that do not, in themselves, absorb energy. The ideal structural weight (or minimum possible weight) of a filament wound pressure vessel has been shown, Reference 10, to be

$$W_{Ideal} = \frac{3\,pV}{\lambda}\,(SF) \qquad (2)$$

where p is the pressure of the contained fluid, V is the volume of the container, (SF) is the factor of safety, and λ is the specific strength of the structural filaments, defined by

$$\lambda = \frac{\sigma_{ult}}{\rho g} \tag{3}$$

σ_{ult} is the ultimate stress of the fibers and ρg is the weight per unit volume. λ has the dimension of length.

The weight of other solid, non-structural items and the inefficiency of the structural design can be accounted for by multiplying Eqn. (2) by a factor $(1 + \alpha)$. The weight of the contained gas can be related to the pressure and volume by means of the gas law, $pV = WRT$. The total weight of a pnematic shock absorber may therefore be expressed as,

$$W = \left(\frac{3\,pV}{\lambda}(1 + \alpha)(SF) + \frac{pV}{RT}\right) \tag{4}$$

pV in the first term may be replaced by $p_g V_o$ where p_g is the gage pressure and V_o is the volume under no load, provided that the peak stress in the wall of the container occurs under no load. This is, fortunately, true under most conditions for a filament-wound toroidal pressure vessel, as will be seen.

The energy absorbed by a pneumatic shock absorber is stored in the gas and also, if the container is strained to a significant degree, in the structural material. An expression for the absorbed energy is

$$E_a = -\int_{V_o}^{V} p\,dV + p_a (V - V_o) + V_s \int_{\epsilon_o}^{\epsilon} \sigma\,d\epsilon \tag{5}$$

The second term accounts for the work done against an external fluid at ambient pressure, p_a. The third term accounts for the energy stored in the volume of structural material, V_s. Ignoring, for the moment, the energy stored in the structural material, the energy absorbed during an isobaric (contant pressure) process is

$$E_a = p_g (V_o - V) \tag{6}$$

so that, if the volume is compressed to zero, the specific energy is, by substituting (4) and (6) into (1):

$$E_s = \frac{1}{\frac{3}{\lambda}(1+\alpha)(SF) + \left(\frac{p_o}{p_g}\right)\frac{1}{RT}} \tag{7}$$

where $p_o = p_a + p_g$, is the absolute pressure at no load.

The energy absorbed during an adiabatic process, again ignoring energy absorbed in the structure, is;

$$E_a = \frac{p_o V_o}{K-1}\left[\left(\frac{V_o}{V}\right)^{K-1} - 1\right] - p_a V_o \left(1 - \frac{V}{V_o}\right) \tag{8}$$

where K is the ratio of specific heats.

The volume ratio of a compressed toroid with rigid hoop restraint is related to the stroke by

$$\frac{V}{V_o} = 1 - \bar{u}^2 \tag{9}$$

where $\bar{u}$ is the ratio of the stroke to the undeflected height of the toroid. The specific energy during an adiabatic process is, by substituting (4), (8) and (9) into (1):

$$E_s = \frac{\frac{1}{K-1}\left[\left(1 - \bar{u}^2\right)^{1-K} - 1\right] - \frac{p_a}{p_o}\bar{u}^2}{\frac{3}{\lambda}\left(1 - \frac{p_a}{p_o}\right)(1+\alpha)(SF) + \frac{1}{RT}} \tag{10}$$

Examination of Eqns. (7) and (10) reveals that the gas constant K and R are significant parameters for a pneumatic shock absorber. The following table gives values for a few gases that have desirable properties:

GAS CONSTANTS

	K	R
Air	1.4	53.3
Hydrogen	1.4	766.8
Helium	1.66	386.3
Argon	1.67	38.7

Specific energies for a toroidal shock absorber under isobaric and adiabatic processes are plotted, respectively, in Figures 2 and 3. In both cases it is assumed that the ambient pressure, p_a, is negligible. A structural material with realistic specific strength is assumed. In the case of adiabatic compression the stroke is assumed to be 90% of the undeflected height because, as will be shown later, the meridional fiber stress is approximately equal to the unloaded fiber stress at that stroke.

The advantages of using lighter gases is indicated in both figures. In addition, the adiabatic process is seen to be considerably more efficient than the isobaric process.

Returning to a consideration of energy stored in the structural material, it is evident from Eqn. (8) that strains large enough to be significant will also change the energy stored in the gas by virtue of an increase in enclosed volume. The volume ratio for a compressed toroid subjected to strain in the meridional fibers is related to stroke, $\bar{u}$, by

$$\frac{V}{V_o} = \frac{(1 - \bar{u}^2) + 2\epsilon(1 - \bar{u})}{1 + 2\epsilon_o} \qquad (11)$$

where ϵ_o is the strain at no load and ϵ is the strain at full compression. It may be observed that if the stroke is large and the initial strain is small the volume ratio is not significantly affected.

Figure 4 shows the relationship between strain and specific stress, $\sigma/\rho g$, for a structural material that is capable of sizeable energy storage. This energy should be included in an evaluation of the potential capability of pneumatic shock absorbers.

Figure 5 shows the results of calculations of specific energy absorption by a toroidal shock absorber using Eqn. (10) and the properties of available materials. In the case of the expendable (Nylon) shock absorber the factor of safety was assumed to be 1.0. The specific energy absorption for competing systems, also shown in Figure 5, is taken from Reference 1.

2.2 Fiber Stress

The meridional tension in a compressed toroid is (see Section 3.3)

$$T_m = p \cdot \frac{h}{2} \tag{12}$$

where h is the compressed height. The relationship between meridional tension and stroke is, therefore

$$\frac{T_m}{T_{m_o}} = \frac{p}{p_o} (1 - \bar{u}) \tag{13}$$

where T_{m_o} is the meridional tension for no load. For an isobaric process meridional tension decreases linearly with stroke. For an adiabatic process

$$p = p_o \left(\frac{V_o}{V}\right)^K \tag{14}$$

so that, using Eqn. (9)

$$\frac{T_m}{T_{m_o}} = \frac{1 - \bar{u}}{\left(1-\bar{u}^2\right)^K} \tag{15}$$

The relationship between hoop tension and stroke is

$$\frac{T_h}{T_{h_o}} = \frac{p}{p_o} (1 - \bar{u}^2) \tag{16}$$

so that, for an adiabatic process

$$\frac{T_h}{T_{h_o}} = \frac{1}{(1 - \bar{u}^2)^{K-1}} \tag{17}$$

The above relationships are plotted in Figure 6 for both isobaric and adiabatic processes. For the isobaric process both components of tension decrease uniformly with stroke. For the adiabatic process the hoop tension increases uniformly with stroke while the meridional tension decreases at first and then rises to exceed the no-load value at a stroke between 80% and 90% of full stroke.

In a meridionally wound toroid, hoop force is carried by concentrated circular rings at the polar circles, see Figure 1, while in a helically, wound toroid hoop force is carried by the inclined fibers. In either case, the fact that hoop force increases uniformly with stroke in an adiabatic process means that additional circumferential reinforcement is required for that process.

2.3 Stroke Efficiency

In many shock absorber applications, the stroke as well as the peak force is limited by design considerations for the configuration as a whole. It is furthermore desirable to absorb as much energy as possible within the limits on peak force and maximum stroke so that the ideal shape for a load-stroke curve is one such that the force rises rapidly (limited by allowable onset rate) to its maximum value and remains constant over the remainder of the stroke.

The relationship between force and stroke for a toroidal shock absorber is (see Eqn. 25):

$$F = \pi^2 \, a \, h_o \, p \, \bar{u} \tag{18}$$

where a is the radius of the polar circle and h_o is the undeflected height

at the toroid. Thus the load-stroke curve is linear under isobaric compression. For adiabatic compression

$$F = \pi^2 a h_o p_o \cdot \frac{\bar{u}}{(1-\bar{u}^2)K} \tag{19}$$

Load stroke curves for both processes are plotted in Figure 7. It is evident that the curves depart considerably from the ideal shape, particularly in the case of adiabatic compression.

Stroke efficiency is defined by the formula

$$\eta = \frac{1}{F_{max} u} \int_o^u F \, dx \tag{20}$$

which may also be written as

$$\eta = \frac{1}{\bar{u}} \int_o^{\bar{u}} \bar{F} \, d\bar{x} \tag{21}$$

where $\bar{F} = F/F_{max}$ and $\bar{x} = x/h_o$. From the form of Eqn. (21) and also from the form of the load-stroke curve, it is evident that the stroke efficiency for isobaric compression is equal to one-half. For adiabatic compression the stroke efficiency is

$$\eta = \frac{1}{(K-1)} \cdot \frac{\left[(1-\bar{u}^2) - (1-\bar{u}^2)K\right]}{2\bar{u}^2} \tag{22}$$

Stroke efficiency curves for toroidal shock absorbers are plotted in Figure 8. Stroke efficiency for the adiabatic process can be improved by using bleed-off valves to control the shape of the load-stroke curve. In Figure 7, for example, the pressure could be permitted to rise adiabatically until the stroke attained 60% of the undeflected height. At this point bleed-off

valves would be forced to open by the increasing pressure so as to maintain the pressure at a constant value. At the end of the stroke, the pressure would be reduced quickly to a low value in order to prevent rebound of the shock absorber.

Another scheme for improving the stroke efficiency of a toroidal shock absorber is shown in Figure 9. The toroid stack is pre-compressed by means of drop cords to provide a rapid onset of force. The pressure then rises adiabatically to a level at which bleed-off valves open and thereafter maintain the pressure at a constant value. A further advantage of the configuration shown in Figure 9 is that the meridional fiber stress is near its minimum value in the no-load condition (see Figure 6). It is, therefore, possible to exploit efficiently the energy-storage capability of the structural fibers and to increase the specific energy of the shock absorber.

3. STIFFNESS PROPERTIES OF A COMPRESSED TOROID

As its name implies, a shock absorber is a highly compliant part of structural system. In order to make engineering calculations concerning the total response of the system, the intrinsic relationships between motions at the points where the shock absorber attaches to the rest of the system and the forces applied to these points should be known. In the case of a toroidal shock absorber, the important motions are the translations and rotations of planes passing through the polar circles of the toroid. Relationships between these motions and applied static forces and moments will be derived in this section, and will be applied in the next section to the computation of the elastic stability of a stack of toroids. In deriving stiffness properties, it will be assumed that the toroid is subjected to large deformation parallel to its polar axis, but that lateral translations and rotations are infinitesimal. This assumption is reasonable since, in most applications, the applied axial force is large compared to lateral forces and moments. A further implied assumption, for the calculation of dynamic response, is that the mass of the toroid may either be neglected or be lumped at its points of attachment to the rest of the system.

3.1 Resistance of a Toroid to Axial Compression

The axial force on a toroid compressed between parallel plates, Figure 10, is equal to the internal pressure multiplied by the footprint area

$$F = p\pi (r_2^2 - r_1^2) \tag{23}$$

Under the assumptions that the fibers are inextensional and without bending stiffness and that the deflected height, h, is small compared to the diameter of the polar circle, 2a, the toroid deforms into a shape with semicircles at the inner and outer meridians such that, in Figure 10,

$$c_1 = c_2 = \frac{\pi}{4} (h_o - h) \tag{24}$$

Substituting $r_1 = a - c_1$ and $r_2 = a + c_2$ into Eqn. (23), we obtain

$$F = p\pi^2 a \cdot (h_o - h) = p\pi^2 a \cdot u \tag{25}$$

The spring constant of the compressed toroid is independent of the stroke, u, and is equal to $p\pi^2 a$.

3.2 Resistance of a Compressed Toroid to Bending

The bending stiffness of a compressed toroid will be computed under the assumption that, θ, the angle between the cover plates is infinitesimal, (see Figure 11). The case of finite rotation is difficult and will not be treated.

The bending moment is equal to the first moment of the pressure acting on the footprint area of the toroid,

$$M = \int_0^{2\pi} \int_{r_1}^{r_2} p\, r^2 \cos\varphi \, d\varphi \, dr = \frac{p}{3} \int_0^{2\pi} (r_2^3 - r_1^3) \cos\varphi \, d\varphi \tag{26}$$

where φ is the azimuth angle to the plane of rotation. From Figure 11

$$r_2 = a + c_2 = a + \frac{\pi}{4}(h_o - h_2) = a + \frac{\pi}{4}(h_o - h + (a + c_2)\,\theta \cos\varphi) \tag{27}$$

and

$$r_1 = a - c_1 = a - \frac{\pi}{4}(h_o - h_1) = a - \frac{\pi}{4}(h_o - h + (a - c_1)\,\theta \cos\varphi) \tag{28}$$

In cubing r_1 and r_2, only the terms that are linearly proportional to θ will be retained. These terms are

$$\text{L. P. } (r_2^3 - r_1^3) = \frac{3\pi}{4}\theta \cos\varphi \left[2a^3 + 6a\left(\frac{\pi}{4}\right)^2 (h_o - h)^2\right] \tag{29}$$

Thus, upon substituting into Eqn. (26) and performing the integration

$$\frac{M}{\theta} = \frac{\pi^2}{2} p a^3 \left[1 + 3\left(\frac{\pi}{4}\right)^2 \left(\frac{h_o - h}{a}\right)^2\right] \tag{30}$$

The second term in this result is negligible for slender toroids, $h_o \ll a$, and for slightly compressed toroids.

3.3 Resistance to Shear of a Toroid with Meridional Fibers, Compressed Between Two Parallel Plates

Consider a section of a flattened cylindrical tube between parallel plates and displace the top plate in the direction of the axis of the tube

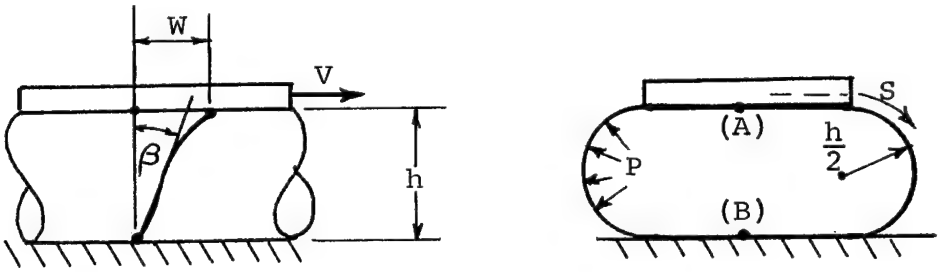

The curved section of the tube has a radius equal to $\frac{h}{2}$. The tensile force in meridional fibers per unit length of tube is

$$T_m = p \cdot \frac{h}{2} \tag{31}$$

The shear force is transmitted by rotation of the fibers out of a meridional plane, i.e.,

$$V = 2\, T_m \sin \beta \tag{32}$$

where β is the angle between the axis of the fiber and a meridional plane. Now from equilibrium considerations the shear force is constant, independent of s, the position on the meridian, so that β is also independent of s. The motion w in the direction of the axis is obtained from

$$w = \int_{s_1}^{s_2} \sin\beta \, ds = \sin\beta \, (s_2 - s_1) \tag{33}$$

If the portions of the fiber in contact with the cover plates do not slip relative to the cover plates, then $s_2 - s_1$ is equal to the length of the curved portion of the meridian and

$$w = \sin\beta \cdot \frac{\pi}{2} \cdot h \tag{34}$$

If, on the other hand, the fiber slips freely such that the shear force is reacted only at points (A) and (B) in the plane of symmetry, then $s_2 - s_1$ is equal to the total length between these points and

$$w = \sin\beta \cdot \frac{\pi}{2} \cdot h_o \tag{35}$$

where h_o is the uncompressed height of the toroid.

The relationship between shear force and displacement is, for the case of no slip,

$$V = 2\,T \sin\beta = 2\left(\frac{p \cdot h}{2}\right) \cdot \frac{2}{\pi} \frac{w}{h} = \frac{2}{\pi}\, p\, w \tag{36}$$

while for the case of free slip

$$V = \frac{2}{\pi}\, p \cdot \left(\frac{h}{h_o}\right) \cdot w \tag{37}$$

In order to apply these results to a toroid they must be integrated over the circumference of the polar circle. The integration factor is

$$\int_0^{2\pi} \sin^2\varphi \cdot a \cdot d\varphi = a \cdot \pi \tag{38}$$

where a is the radius of the polar circle of the toroid and φ is the azimuth angle from the direction of the applied shear force. Thus, the relationship

between shear force and lateral translation for the complete toroid is, for the case of no slip

$$V = 2\,a\,p \cdot w \tag{39}$$

while for the case of free slip

$$V = 2\,a\,p\,\frac{h}{h_o}\,w \tag{40}$$

It must be pointed out that the above results are not directly related to the shear stiffness in the ordinary sense of beam theory. They refer only to the condition where the top and bottom plates are held rigidly parallel by some external means and are compressed together by an external force. The significance of these statements is examined in Section 4.

3.4 Summary of Results

The stiffness relationships that have been derived for a meridionally wound toroid are summarized as follows:

Axial compression

$$F/u = \pi^2\,a\,p \tag{41}$$

Bending

$$\frac{M}{\theta} = \frac{\pi^2}{2}\,a^3\,p\left[1+3\left(\frac{\pi}{4}\right)^2\left(\frac{u}{a}\right)^2\right] \tag{42}$$

Shear with parallel cover plates, ($\theta = 0$)

$$\frac{V}{w} = 2\,a\,p, \text{ for no slip} \tag{43}$$

$$\frac{V}{w} = 2\,a\,p\left(1-\frac{u}{h_o}\right) \text{ for free slip} \tag{44}$$

In all cases stiffness is directly proportional to internal pressure. The primary geometric parameter controlling stiffness is the radius of the polar circle, while the uncompressed height of the toroid, h_o, and the stroke, u, enter to a lesser extent.

4. BUCKLING OF TOROID STACKS

The susceptibility of most gas bags to elastic instability is one of their more objectionable features when considered as impact absorbing devices. The toroidal container is an exception, inasmuch as it shows relatively good resistance to buckling. An approximate theoretical analysis of the buckling of toroid stacks follows. Confirming experiments are described in Section 5.

The buckling of a stack of filament-wound toroids under concentrated end loads is similar to the Euler buckling of a continuous column except that

1. Shear compliance may be relatively more significant and cannot be ignored.
2. If the number of toroids in the stack is small, treatment of the stack as a continuous column may lead to significant error. This is the reverse of the error introduced by using finite difference methods to treat a continuous system.

In calculating its buckling load, the stack of toroids will be treated as a continous column, making due allowance for the above differences. Shear compliance will be considered first.

The resistance to lateral load of a meridionally-wound toroid placed between parallel plates is given by Eqns. (43) and (44). If, instead of lying in meridional planes, the fibers form a double helical wrap with an average angle β_o between the fibers and meridional planes (see Figure 1b), it may be shown (Ref. 11) that the resistance to lateral force is given by

$$\frac{V}{w} = \pi a \cdot E \cdot \frac{d^2}{h_o \ell_f} \sin \beta_o \cos \beta_o \qquad (45)$$

where, in addition to previously defined symbols,

E = Young's modulus of fibers

d = fiber diameter

ℓ_f = distance between fiber intersections

In view of the very large ratio of E to p in practical applications, the resistance of a helically-wound toroid to lateral force will be considered to be infinite compared to its resistance to bending.

The values obtained from Eqns. (43), (44) and (45) for V/w should not be identified directly with shear stiffness. They refer rather to the case of a toroid between plates that are kept parallel by external constraints, as depicted below

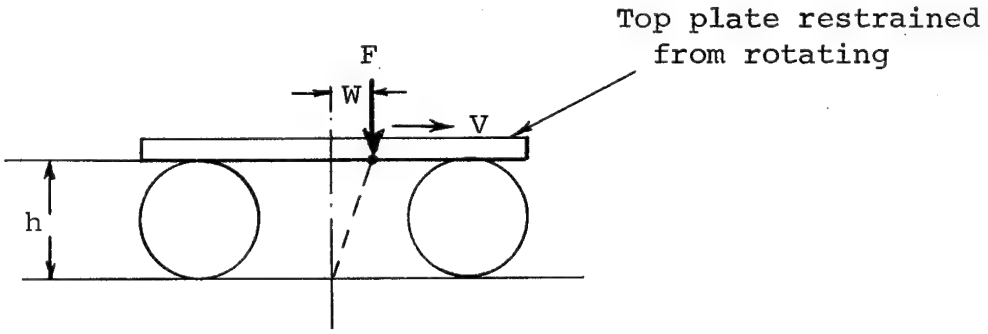

Since we are interested in deriving the equivalent beam properties of a toroid, the results for this configuration should be compared with corresponding results for a column with ends restrained from rotation. For this purpose, resolve the applied load into a component directed toward the center of the base of the column and a component parallel to the top surface. The first component has negligible effect for a differentially short column. The net lateral force on the top plate is, for small motions

$$V_o = V + F \cdot \frac{w}{h} \tag{46}$$

The lateral deflection of the equivalent column with parallel ends is

$$w = V_o \left[\frac{h}{KAG} + \frac{1}{12} \frac{h^3}{EI} \right] \tag{47}$$

The equivalent shear stiffness, obtained by combining Eqns. (4) and (5) is

$$\frac{1}{KAG} = \left[\frac{1}{\frac{hV}{w} + F} - \frac{h^2}{12\,EI}\right] \tag{48}$$

$\frac{V}{w}$ is given by Eqns. (43), (44), or (45). The bending stiffness, M/θ, of a toroid is derived in Section 3.2. For slender toroids in general, or for any toroid that is only slightly compressed,

$$EI = \frac{Mh}{\theta} = \frac{\pi^2}{2}\, p\, a^3\, h \tag{49}$$

The bending stiffness of fat, highly compressed toroids is somewhat larger. Eqn. (49) will be used in subsequent work.

The bending load of an Euler column including the effect of shear flexibility is

$$F = \frac{1}{\frac{1}{KAG} + \left(\frac{2\ell}{m\pi}\right)^2 \cdot \frac{1}{EI}} \tag{50}$$

where ℓ is the length of the column and m is the fixity index. The length of the column, ℓ, is equal to nh where n is the number of toroids in the stack. For common end conditions

m = 1 for a cantilever column

m = 2 for a simply-supported column

m = 4 for a column with built-in ends.

The analysis has been carried out for the conditions to which Eqns. (43) and (44) apply and also to the condition for which $\frac{w}{V} = 0$, which approximates the helically wound toroid. In the analysis, use is made of the relationship between the compressive load, F, and the axial deflection, u, of a single toroid, derived in the preceding section

$$F = p \cdot a \cdot \pi^2 \cdot u \tag{51}$$

Examination of the preceding equations reveals that F, KAG, and EI are all directly proportional to the internal pressure, p. Thus, pressure is eliminated as a parameter in the buckling criterion, Eqn. (50), and it may be concluded that a given toroid stack will buckle at some deflected height, regardless of the internal pressure. Eqn. (50) may be used to obtain a relationship between the deflection and the physical parameters that describe the stack of toroids. The general form of the relationship obtained by substituting Eqns. (48), (49) and (51) into Eqn. (50) is

$$\frac{2\,h_o^2}{a^2}\left[\left(\frac{2n}{m\pi}\right)^2 - \frac{1}{12}\right] = f(\bar{u}) \tag{52}$$

where, for a helically-wound toroid with $\frac{w}{V} = 0$:

$$f(\bar{u}) = \frac{1}{\bar{u}(1-\bar{u})} \tag{53}$$

for a meridionally-wound toroid with no slip between contacting fibers:

$$f(\bar{u}) = \frac{1}{1-\bar{u}}\left[\frac{1}{\bar{u}} - \frac{1}{\frac{2}{\pi^2} + \left(1 - \frac{2}{\pi^2}\right)\bar{u}}\right] \tag{54}$$

while, for a meridionally-wound toroid with free slip between contacting fibers

$$f(\bar{u}) = \frac{1}{1-\bar{u}}\left[\frac{1}{\bar{u}} - \frac{1}{\bar{u} + \frac{2}{\pi^2}(1-\bar{u})^2}\right] \tag{55}$$

The above results are plotted in Figure 12. As mentioned earlier, reverse finite difference error can be expected due to the application of a continuum formula (Eqn. (50)) to a lumped structure. If $\frac{n}{m} \leq 1$, then $\left(\frac{2n}{\pi m}\right)^2 = .405\left(\frac{n}{m}\right)^2$ should be replaced by $\left(\frac{1}{3}\right)\left(\frac{n}{m}\right)^2$ in Eqn. (52). The error in Eqn. (52) is small for larger values of n/m.

The results shown in Figure 12 may be put into a more convenient form by noting that $nh_o/2a$ is the aspect ratio,(i.e., the ratio of total height to polar diameter) of the unloaded stack. Neglecting the term 1/12 compared to $\left(\frac{2n}{m\pi}\right)^2$,

the result shown in Figure 13 is obtained for a simply-supported stack. For a stack with fixed ends, the aspect ratio should be doubled, while for a cantilever stack, it must be halved.

Figure 13 shows that, from a design viewpoint, the critical buckling parameters of a stack of toroids are the aspect ratio of the unloaded stack and the stroke. It is of interest to observe that the permissible aspect ratio of a helically-wound toroid stack does not decrease with increasing stroke, if the stroke exceeds one-half of the undeflected height. In addition, toroid stacks with meridionally-wound fibers have a much lower permissible aspect ratio due to their substantial shear compliance.

The manner by which the experimental points plotted in Figures 12 and 13 were obtained is discussed in the next section.

5. EXPERIMENTAL PROGRAM

An experimental program was undertaken to substantiate theoretical predictions of stiffness and buckling behavior. The configuration employed in stiffness tests is shown in Figure 1a. It consists of an automotive innertube covered by a meridional wrap of Dacron fibers. Two fiberglass hoops are located at the polar circles. The meridional fibers are embedded in a knitted mesh of lightweight fibers (barely visible in the photograph) to keep them from slipping. Dimensional properties of the specimen are as follows:

Polar diameter: 12"

Cross-sectional diameter: 4.6"

Filamentary material: 80 lb. Dacron, twisted

Total number of fibers: inner half 242
outer half 425

Total weight, including innertube: 1.4 lb

Ultimate pressure (designed): 300 psi.

The toroid was subjected to pure compression, combined compression and bending, and combined compression and shear tests. The test apparatus for the combined compression and bending test is shown in Figure 14. The compressed height of the center of the toroid was adjusted to the desired value by means of turnbuckles. Bending moment was provided by means of an eccentric weight.

A sketch of the test apparatus for the combined compression and shear test is shown in Figure 15. In this case, the cables and turnbuckles are used to prevent rotation of the cover plate as well as to enforce the desired compressed height. Thus, the results of theoretical analysis (Eqns. (43) and (44)) apply directly to the test condition.

Typical comparisons of test results with theoretical stiffness predictions are shown in Figures 16, 17 and 18. In all cases, but particularly in the

combined compression and shear tests, hysteresis due to fiber slippage and other frictional effects is evident. Nevertheless, the agreement is sufficiently good to validate the theory for design calculations.

The configuration employed in buckling tests is shown in Figure 19. It consists of a stack of four toroids, each of which is substantially identical to the one used in stiffness tests. The meridional fibers of adjacent toroids are interwoven around fiberglass hoops to provide structural continuity.

Results for a cantilever test are shown in Figure 21, where the reciprocal of the angular rotation of the top plate is plotted against stroke. Due to unavoidable misalignments and non-linear effects, the angular rotation does not indicate an especially sharp increase in the neighborhood of the theoretical buckling height. Nevertheless, an extrapolation to zero of the (nearly) linear portion of the plot of $1/\Delta\theta$ vs stroke gives a very good comparison with theory.

Results obtained for a simply-supported test are shown in Figure 22. The simply-supported condition was simulated by tying the mid-points of the cover plates together with a stranded steel cable. These experimental results also indicate a rather gradual collapse of the toroid stack, but extrapolation of $1/\Delta\theta$ gives reasonably good agreement with theory.

In a third set of tests, the buckling limit with fixed ends was determined. The onset of buckling with deflection was rather gradual with the development of large lateral deflections near 50% stroke. A photograph of the buckled stack is shown in Figure 20.

Experimentally determined points are plotted for comparison with theory in Figures 12 and 13. The agreement is sufficiently good to validate the theory for design calculations. The experimental value for the toroid stack with fixed ends (bottom point in Figure 12) indicates that it is best to assume that fibers placed in contact by compression slip freely.

6. CONCLUSIONS

The conclusions of the present study may be summarized as follows:

1. The specific energy absorption of a pneumatic shock absorber, employing an adiabatically-compressed gas, is potentially quite large compared to competing systems, as shown by Figures 2 and 3

The specific energy absorption can be substantially increased by exploiting the stretch capability of highly ductile fibers, such as Nylon.

2. Light gases, particularly helium, should be used in pneumatic shock absorbers because they increase specific energy absorption without penalty.

3. There is a need to develop designs that improve the stroke efficiency of toroidal shock absorbers without severely penalizing specific energy absorption; see Figures 7 and 8.

4. Deflections due to lateral load can be accurately predicted by the theory presented in this report; see Figures 16, 17 and 18.

5. The onset of buckling can be adequately predicted by the theory presented in this report; see Figures 12 and 13. The primary parameters influencing buckling are the aspect ratio of the toroidal stack and the shear flexibility. In applications where buckling is critical, helical rather than meridional fiber patterns should be used in order to reduce shear flexibility.

REFERENCES

1. Esgar, Jack B.: "Survey of Energy-Absorption Devices for Soft Landing of Space Vehicles," NASA TN D-1308, June 1962.

2. Esgar, Jack B., and Morgan, William C.: "Analytical Study of Soft Landings on Gas-Filled Bags," NASA TR R-75, March 1960.

3. Turnbow, James W., and Ogletree, William B.: "The Energy-Dissipating Characteristics of Airbags," The University of Texas, Structural Mechanics Research Laboratory, Austin, Texas, August 1959.

4. McGehee, John R., and Hathaway, M. E.: "Landing Characteristics of a Re-Entry Capsule with a Torus-Shaped Air Bag for Load Alleviation," NASA TN D-628, November 1960.

5. Fisher, Lloyd J., Jr.: "Landing-Impact-Dissipation Systems," NASA TN D-975, December 1961.

6. Stubbs, Sandy M. and McGehee, John R.: "Investigation of the Landing Characteristics of a Re-Entry Vehicle Having a Canted Multiple-Air-Bag Load-Alleviated System," NASA TN D-1934, August 1963.

7. McGehee, John R., and Vaughan, V. L., Jr.: "Model Investigation of the Landing Characteristics of a Re-Entry Spacecraft with a Vertical-Cylinder Bag for Load Alleviation," NASA TN D-1027, March 1962.

8. Schuerch, H., Burggraf, O., and Kyser, A.: "A Theory and Applications of Filamentary Structures," NASA TN D-1692, December 1962.

9. Schuerch, H., and Burggraf, O.: "Analysis of Axisymmetric Rotating Pressurized Filamentary Structures," NASA TN D-1920, May 1963.

10. Kyser, A. C.: "Design and Performance of Isotensoid Pressure Vessels," Astro Research Corporation, Report ARC-R-80, February 1963.

11. "Analysis of Torus Spring Assembly," Astro Research Corporation, Report ARC-R-151, May 29, 1964.

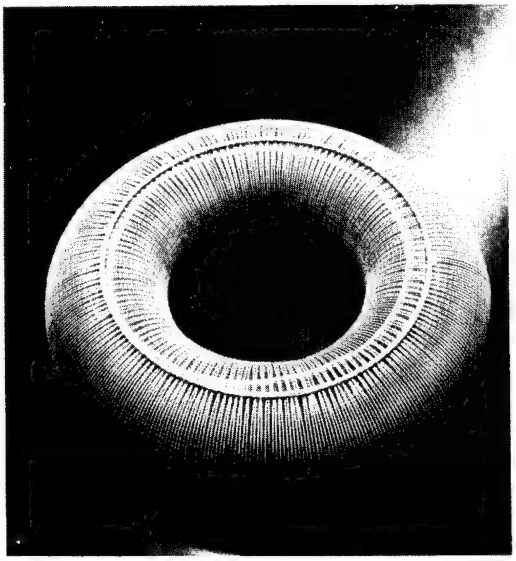

(a) Toroid With Meridional Fibers

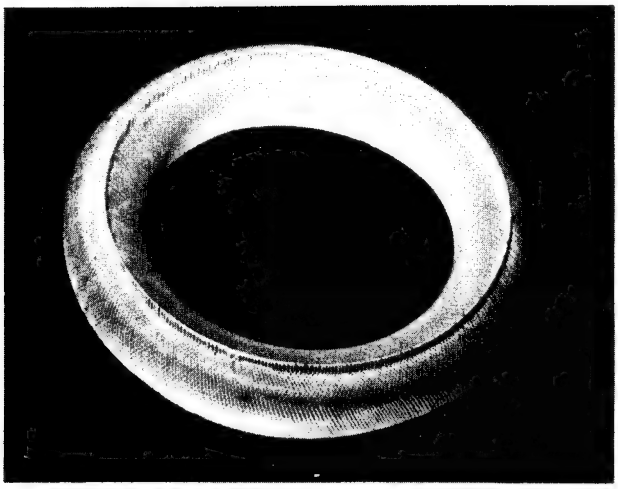

(b) Toroid With Helical Fibers

Figure 1 Filament-Wound Toroids

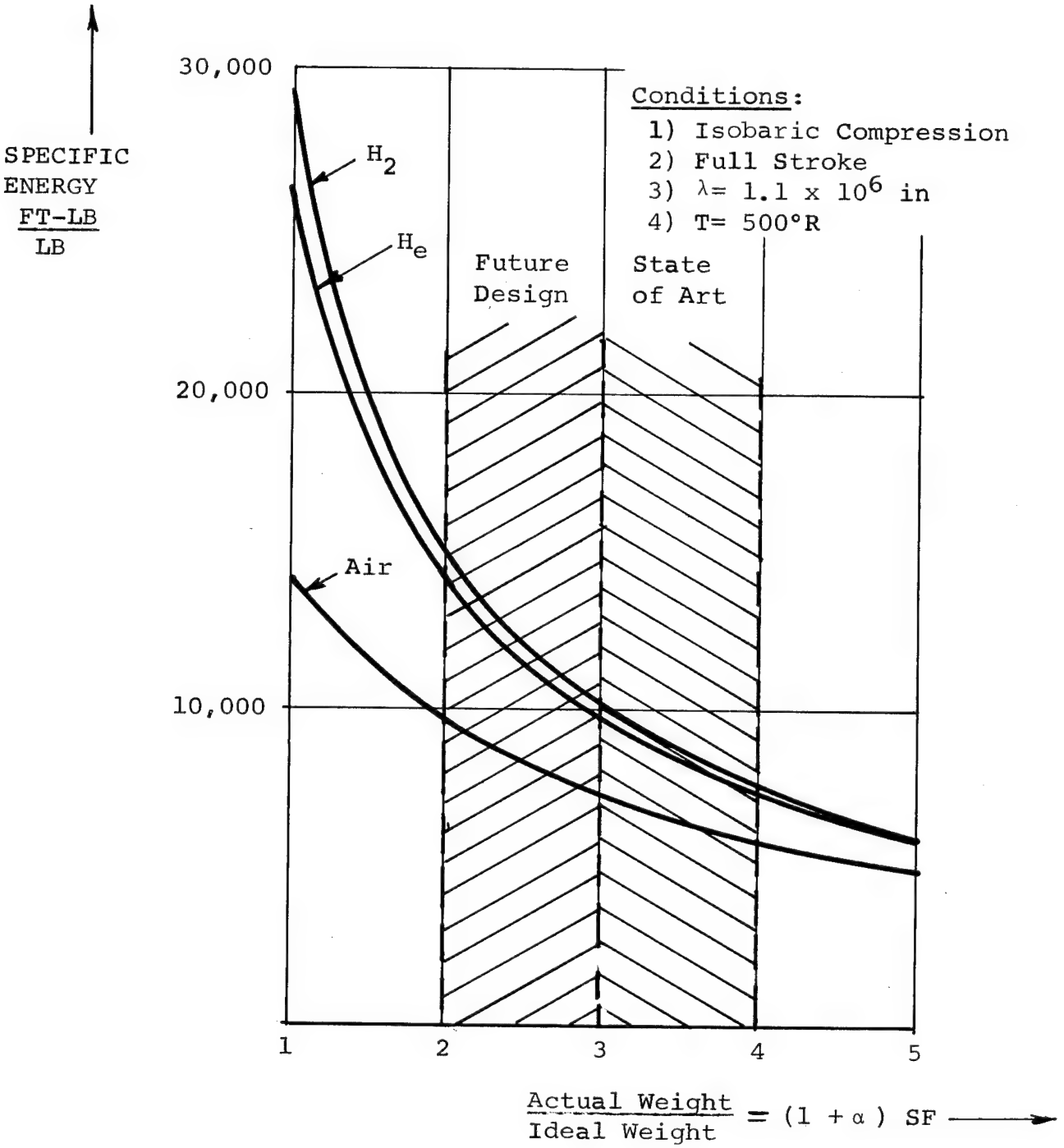

Figure 2 Energy Per Unit Weight Stored in Gas

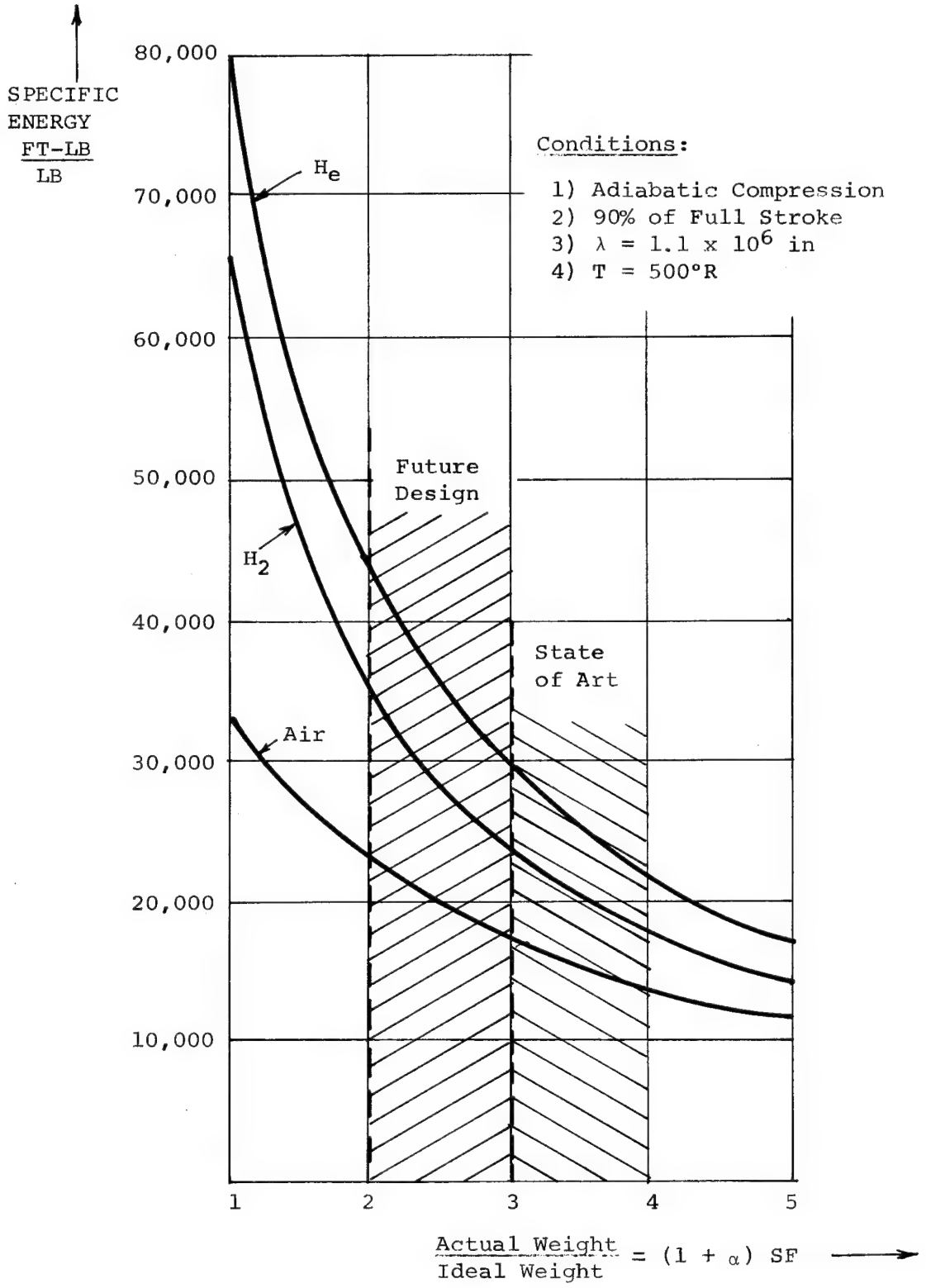

Figure 3 Energy Per Unit Weight Stored in Gas

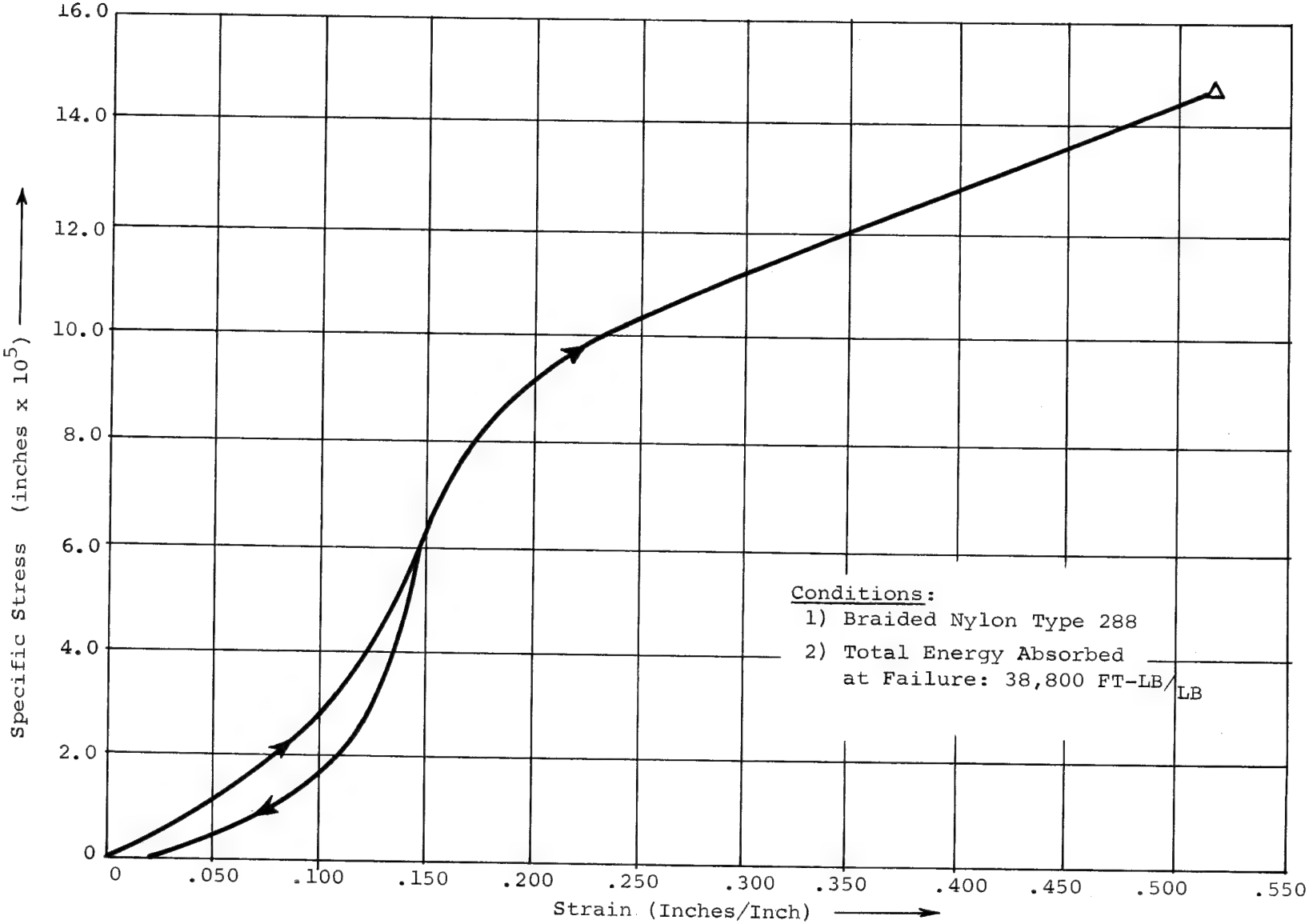

Figure 4 Specific Stress vs. Strain for Braided Nylon

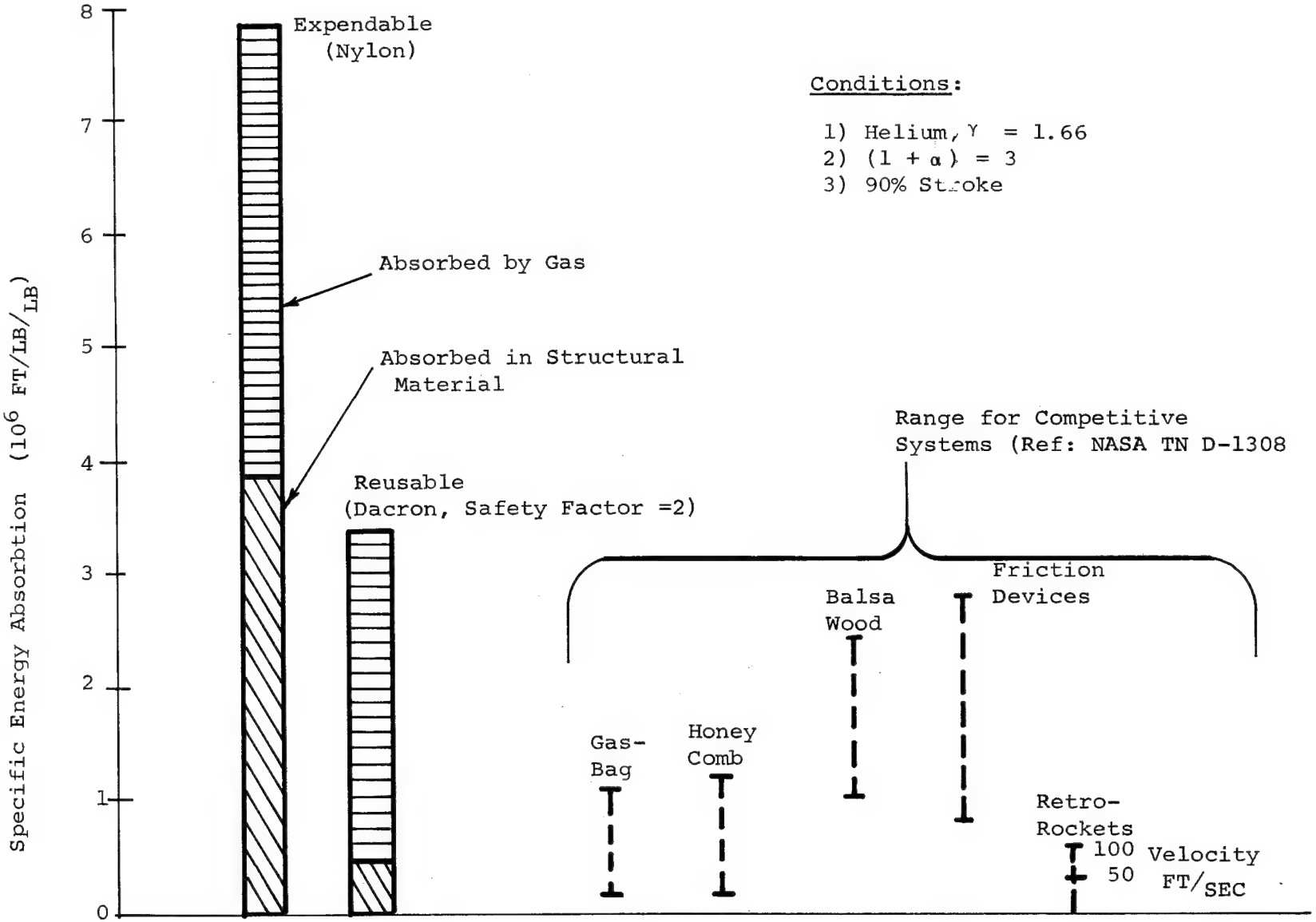

Figure 5 Specific Energy Absorbtion for Torus Stack Shock Absorber

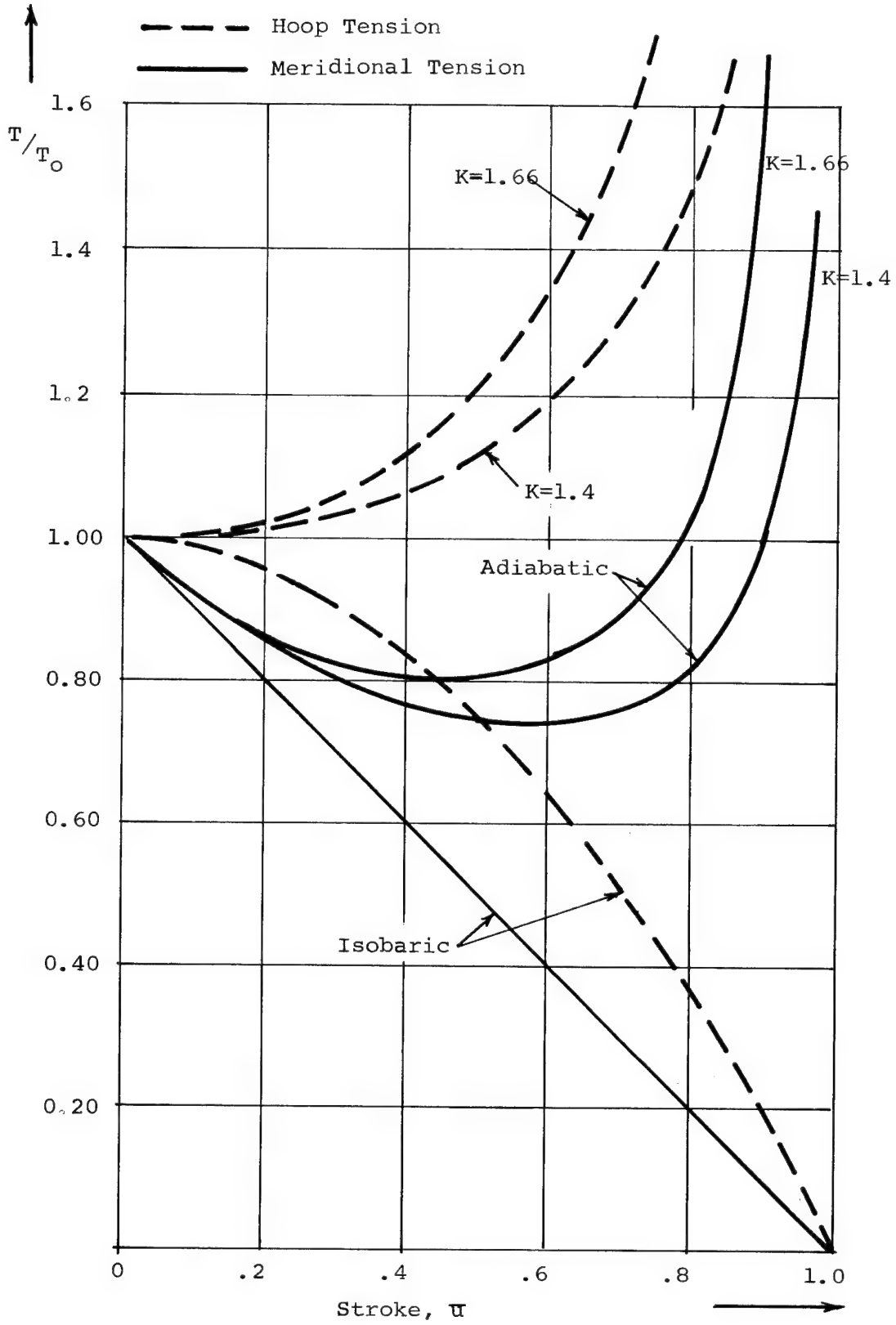

Figure 6 Fiber Tension vs Stroke

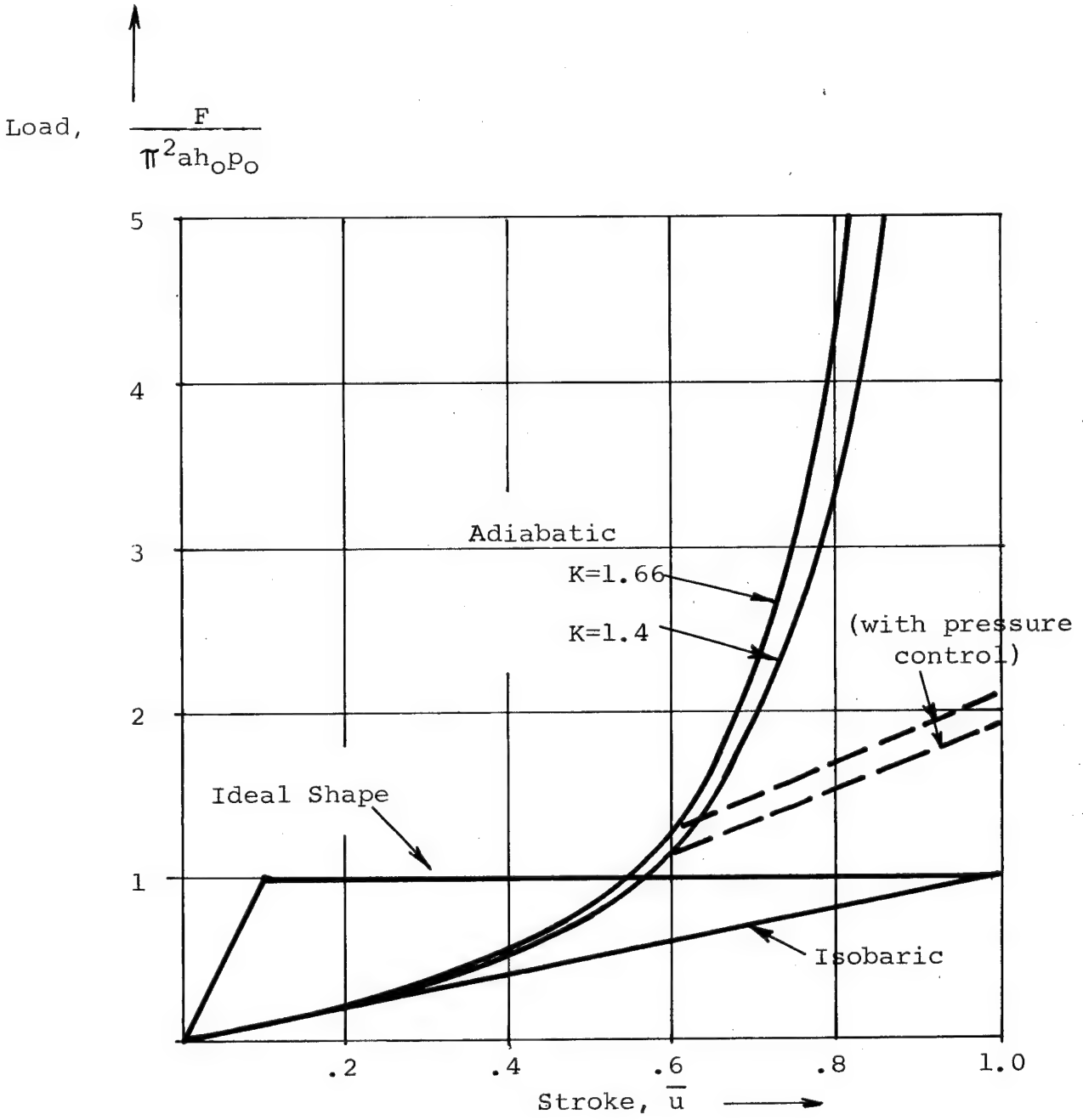

Figure 7 Load vs Stroke for Toroidal Shock Absorbers

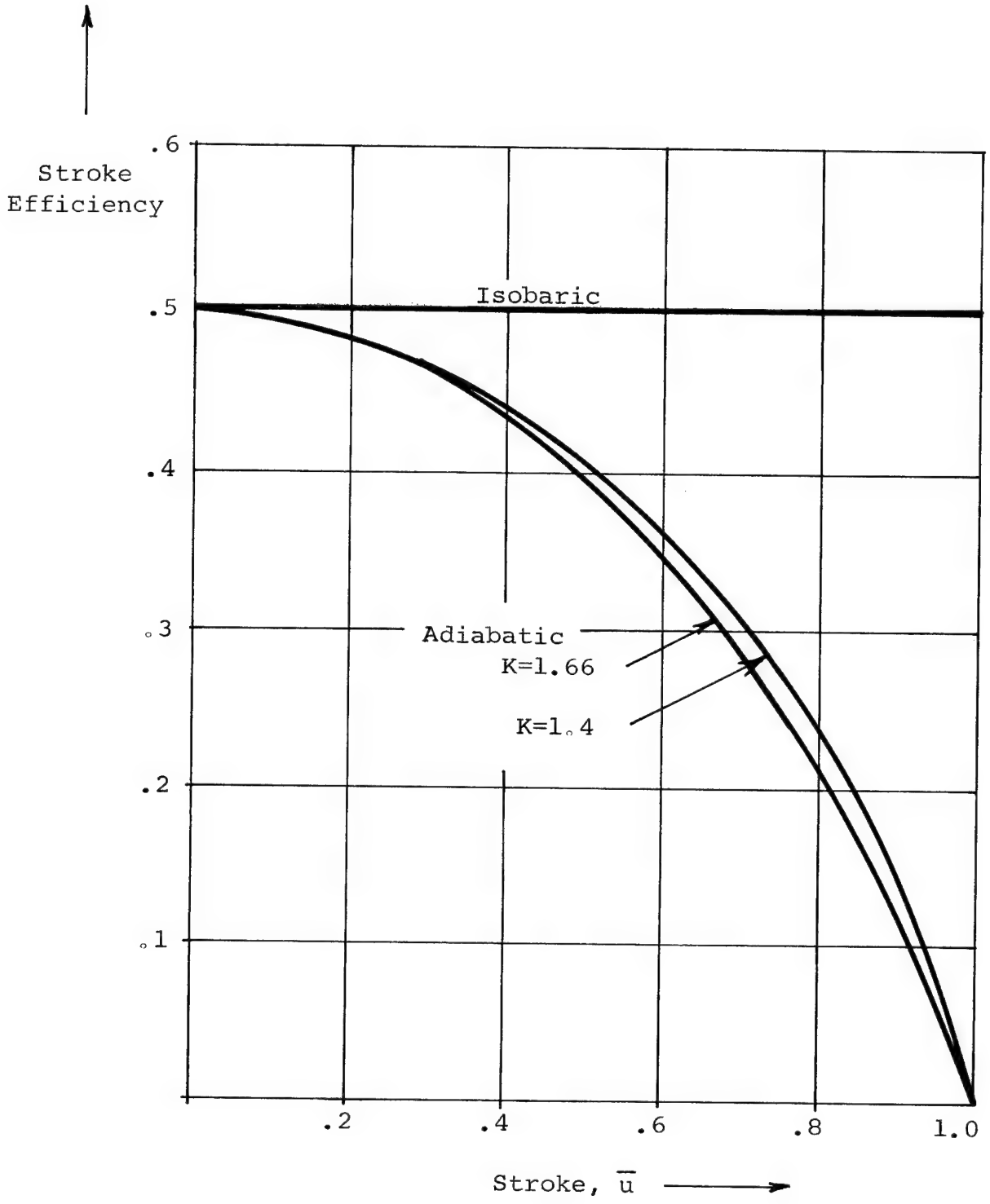

Figure 8 Stroke Efficiency vs Stroke for Toroidal Shock Absorbers

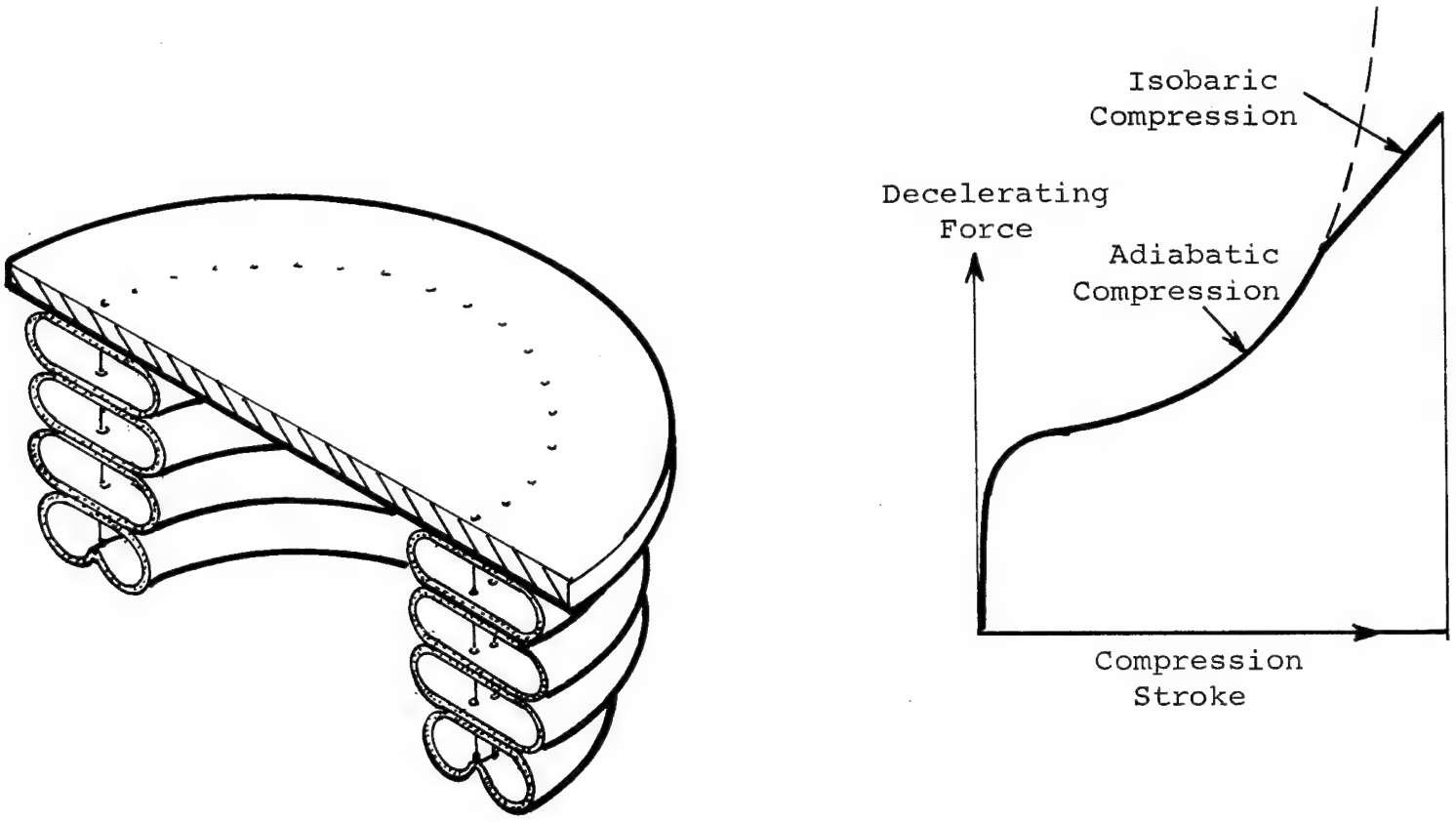

Figure 9 Pre-Compressed Toroid Stack for Best Stroke Efficiency

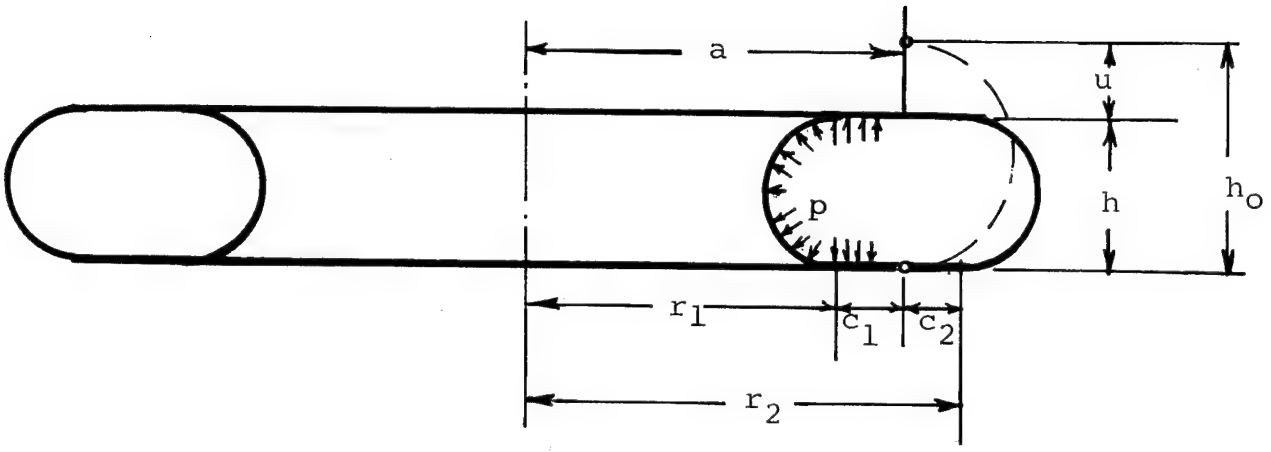

Figure 10 Toroid Under Axial Compression

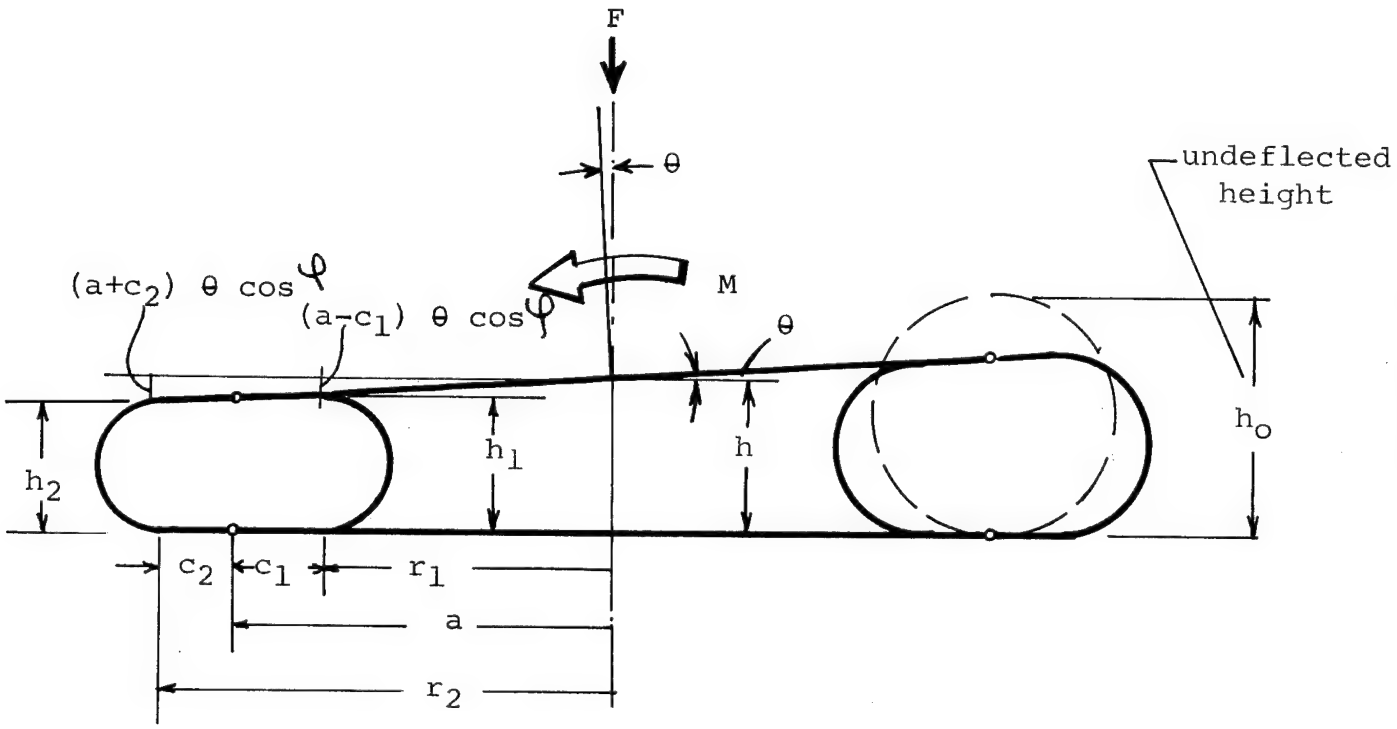

Figure 11 Toroid Under Compression and Bending

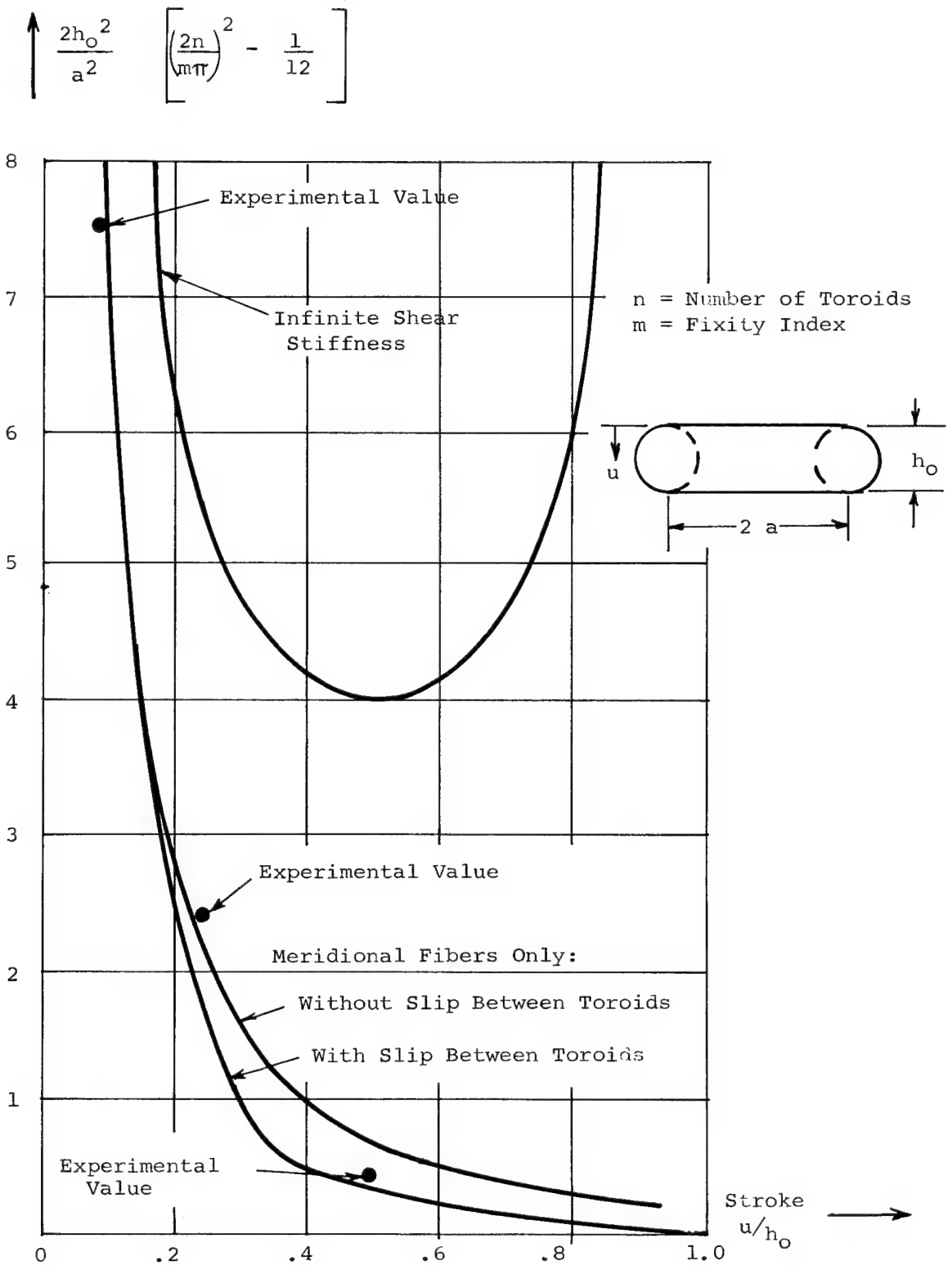

Figure 12 Buckling Coefficient for a Stack of Slender Toroids

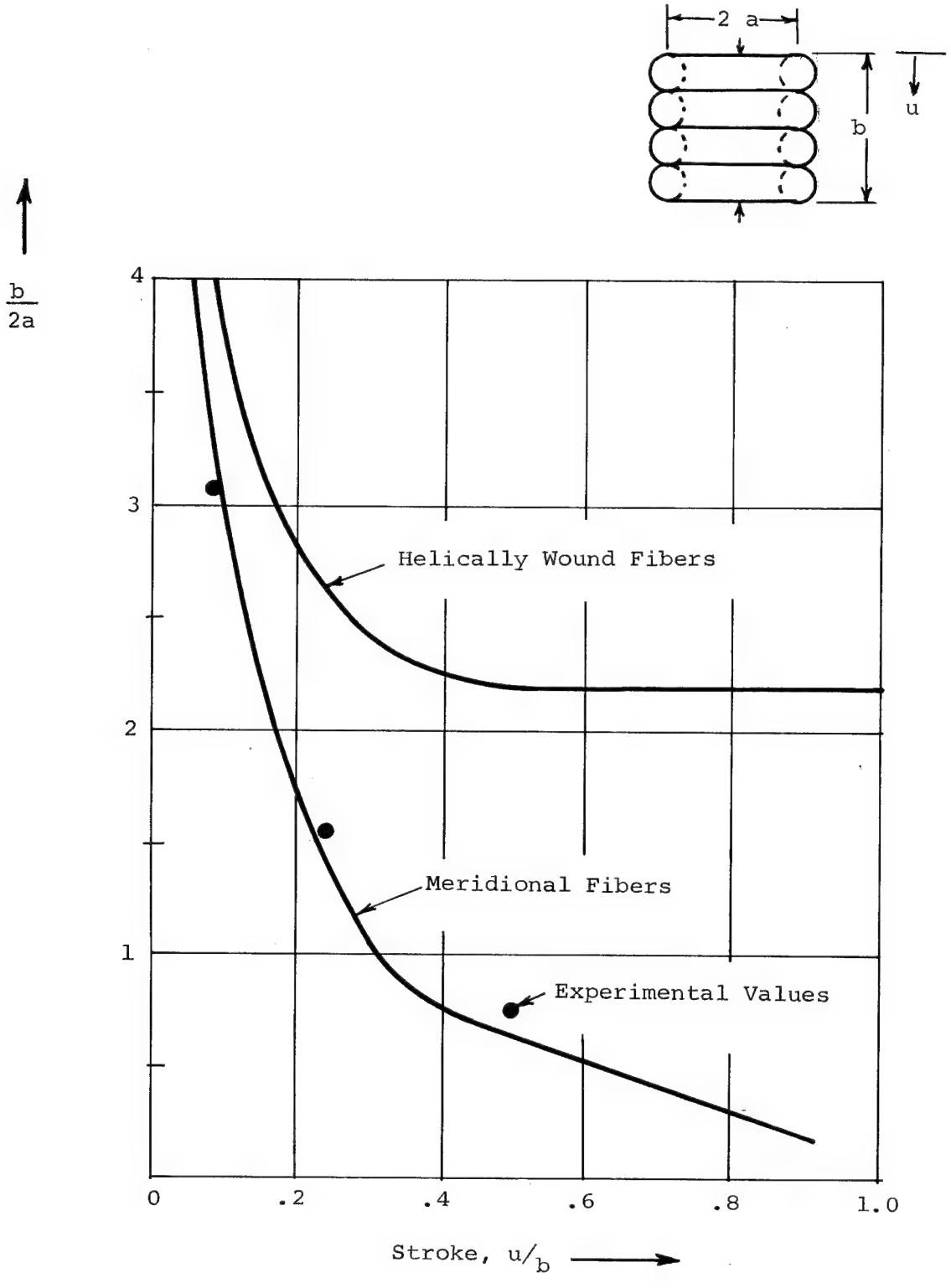

Figure 13 Critical Aspect Ratio for Buckling of a Simply Supported Stack of Toroids

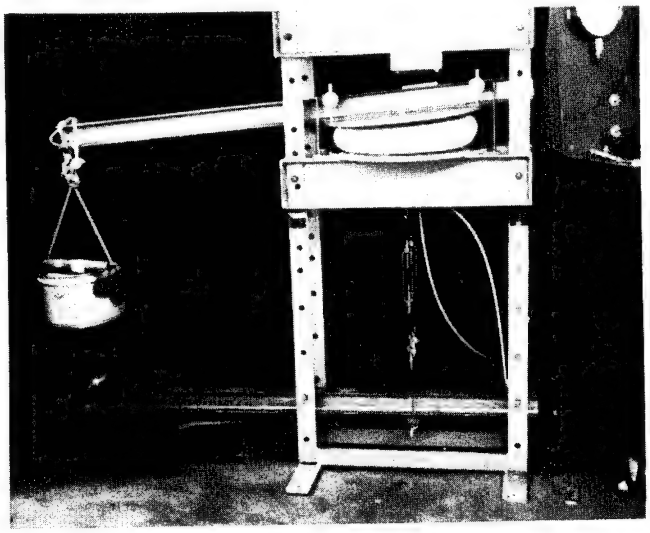

Figure 14 Meridionally Wound Toroid Under Compression and Bending

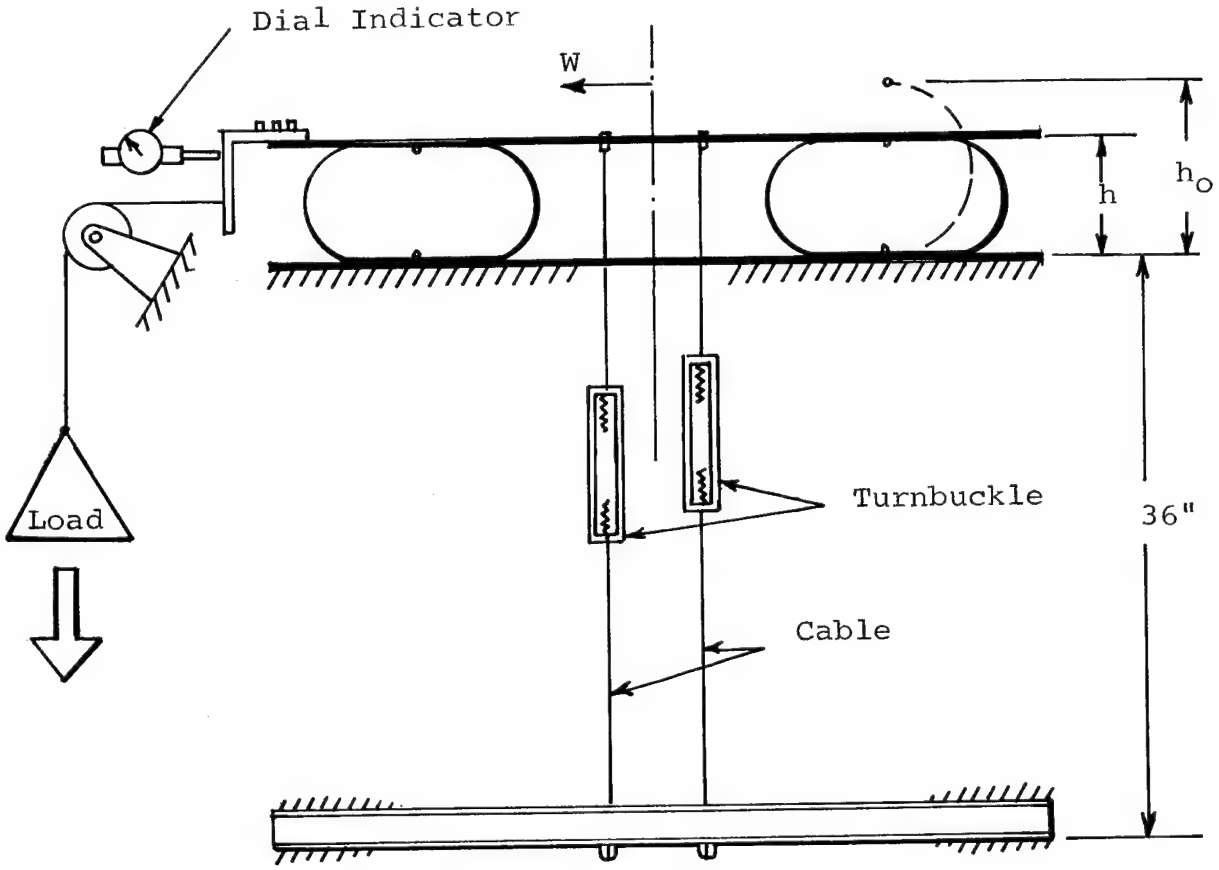

Figure 15 Meridionally Wound Toroid Under Compression and Shear

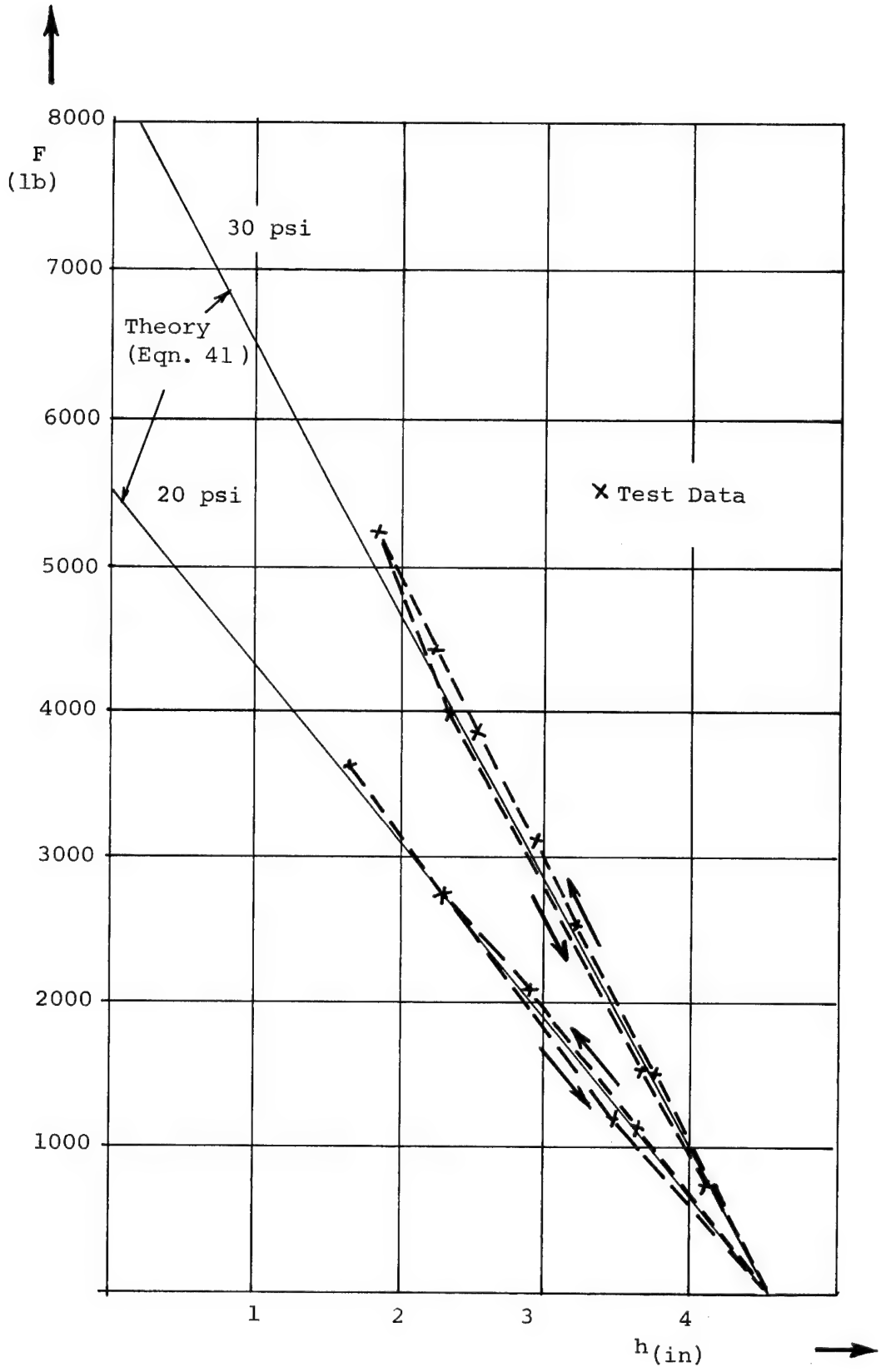

Figure 16 Pure-Compression Test Results

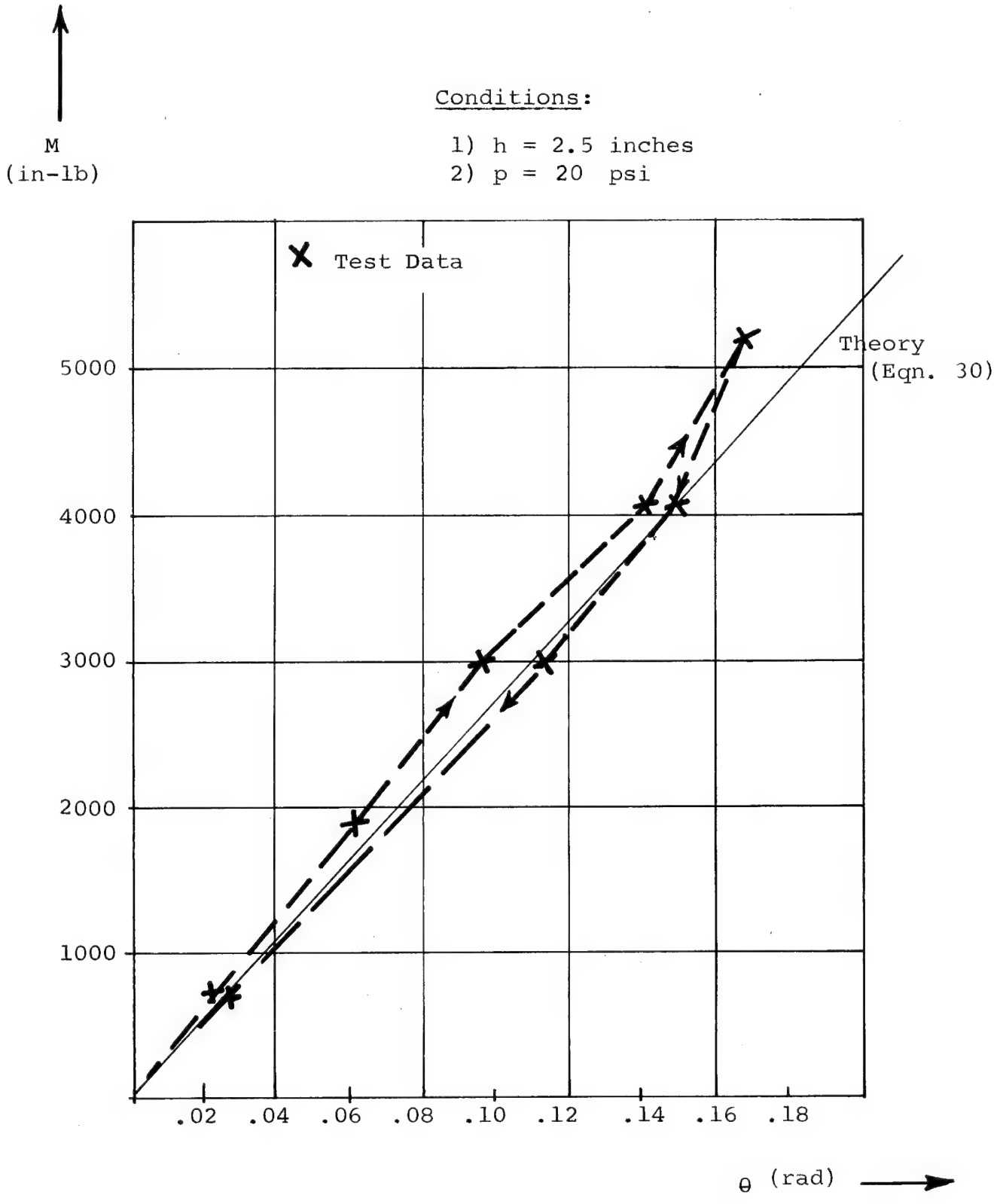

Figure 17 Combined-Compression-and-Bending Test Results

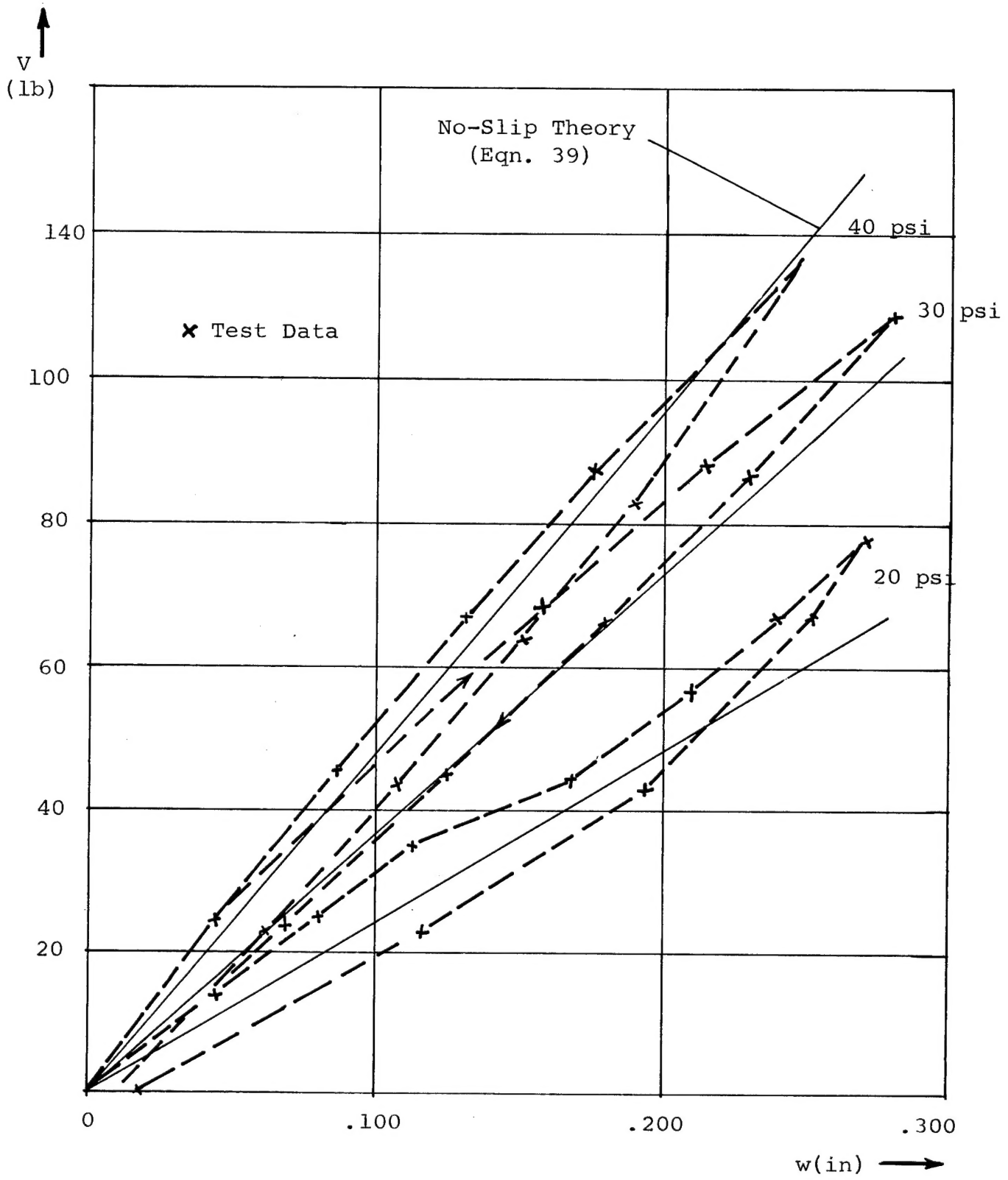

Figure 18 Combined-Tension-and-Shear Test Results

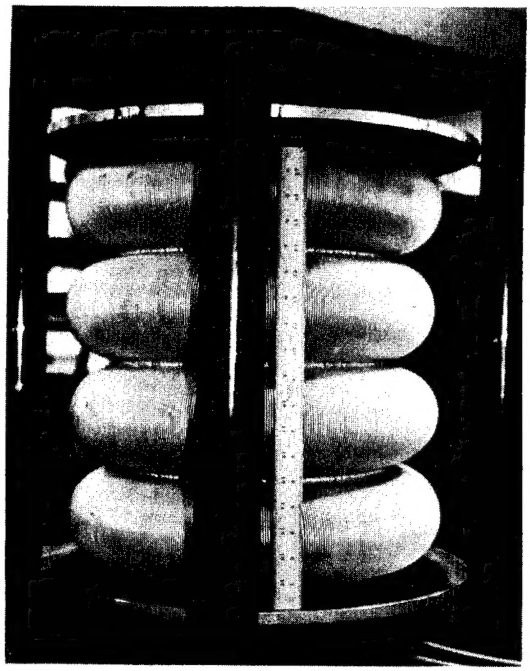

Figure 19 Toroid Stack Before Compression

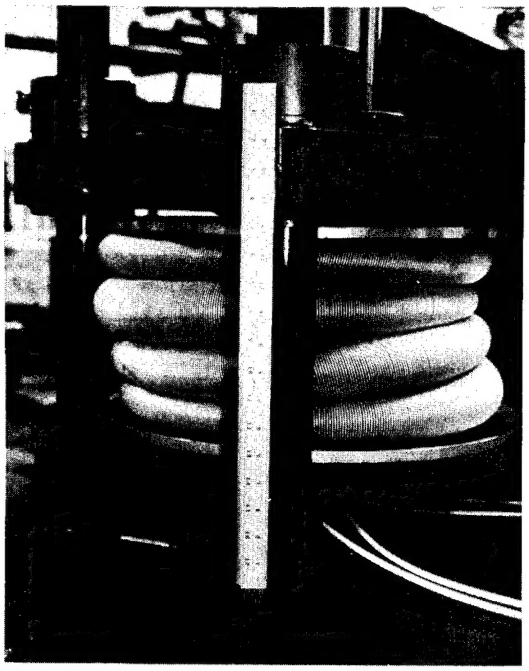

Figure 20 Toroid Stack After Compression Ends Fixed

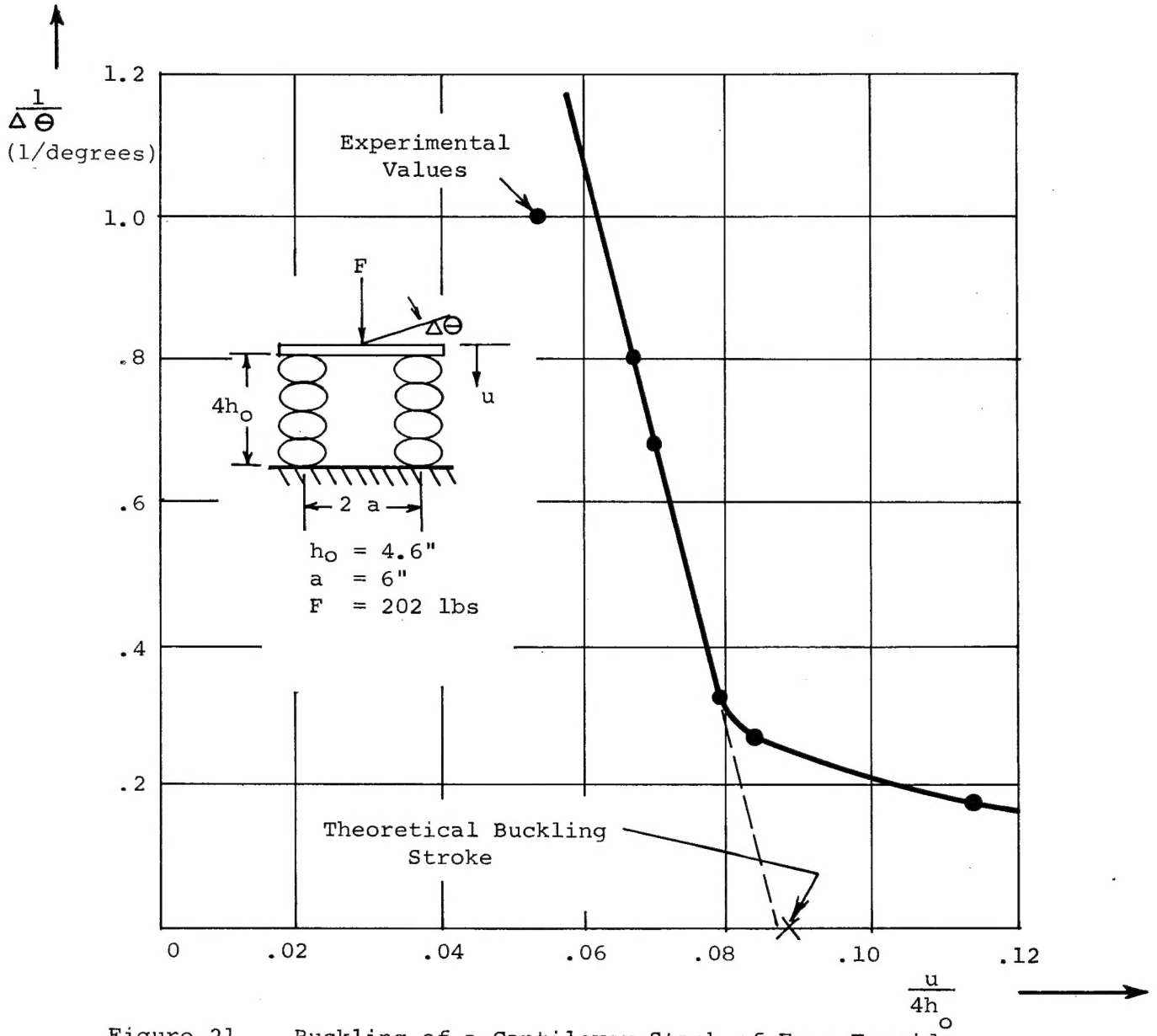

Figure 21 Buckling of a Cantilever Stack of Four Toroids

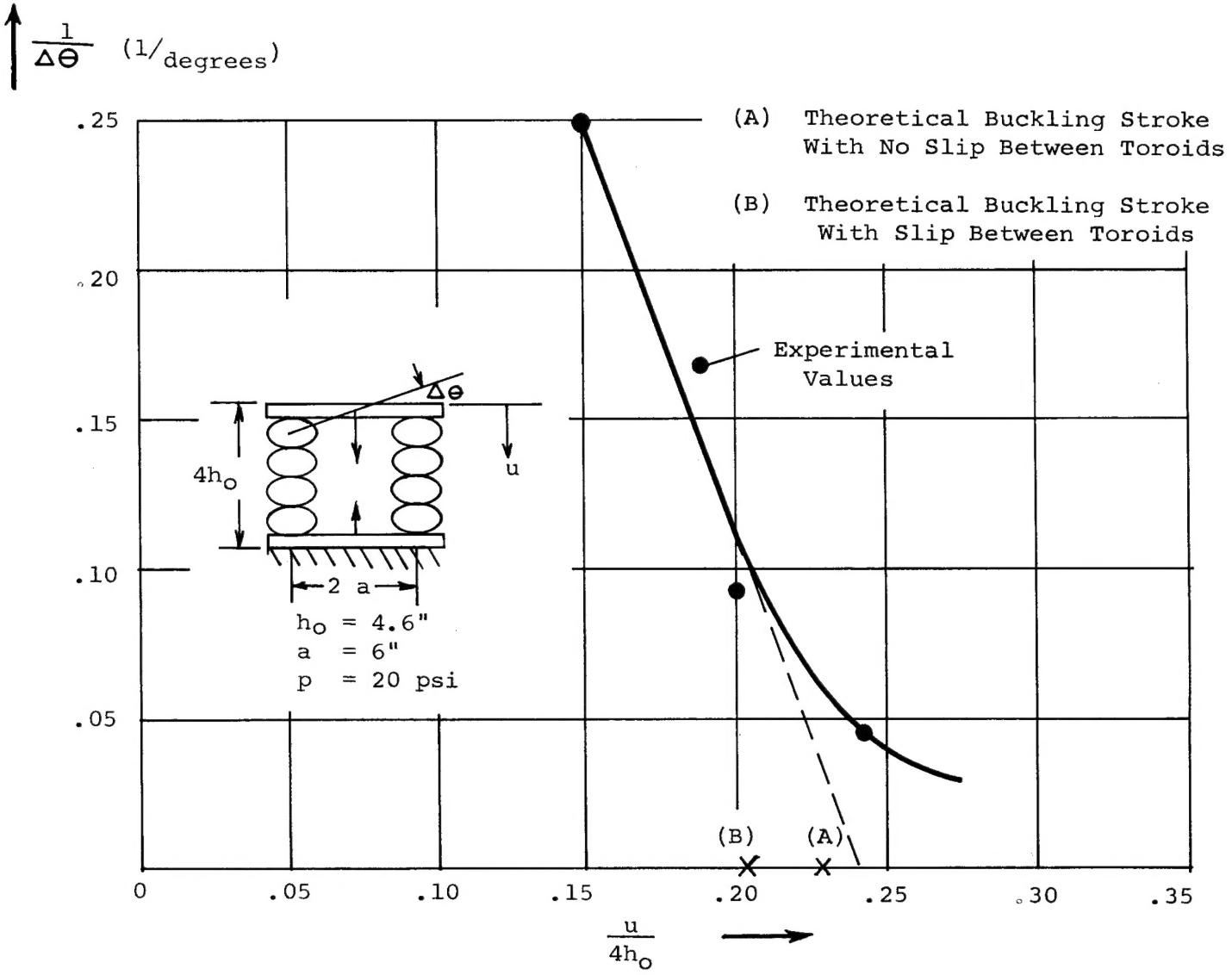

Figure 22 Buckling of a Simply Supported Stack of Four Toroids